Informatics in Medicine Unlocked 30 (2022) 100940

Contents lists available at ScienceDirect

Informatics in Medicine Unlocked

journal homepage: www.elsevier.com/locate/imu

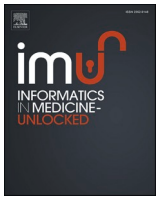

IRlab - Platform for thermal video analysis in evaluation of peripheral thermal behavior and blood perfusion

Tomppa Pakarinen [a,*], Niku Oksala [a,b], Antti Vehkaoja [a]

[a] Faculty of Medicine and Health Technology, Tampere University, Tampere, Finland
[b] Vascular Surgery and Procedural Radiology, Tampere University Hospital, Tampere, Finland

ARTICLE INFO

Keywords:
Thermal imaging
Angiosome
Peripheral blood flow
Perfusion
Matlab

ABSTRACT

Background and objectives: Dynamic thermal imaging in medicine has several advantages in comparison to static thermal image analysis and has potential as a novel patient assessment method e.g. in the area of vascular surgery. Since dynamic thermal imaging has become in the scope of research only during the last decade, the computational available analysis methods are often lacking or not existing. Most of the published software is not available to the research community or are behind a paywall. IRlab provides an easy-to-use dynamic thermal video processing and analysis platform, freely accessible to researchers.

Methods: IRlab is programmed in Matlab R2020b. Computational tools for dynamic analysis are divided into spatio-temporal and spectral methods, where spatio-temporal methods consist of region of interest delineation tools, thermal modulation analysis, standard thermal measures such as median, maximum, minimum and deviation values, and subtraction and gamma maps. Spectral methods include spectral band power, spectral flow, and wavelet analysis tools. Preliminary data of a single healthy subject was analyzed with the program as a sample run.

Results: IRlab provides a platform for lower limb thermal image and video analysis with a clear workflow and variety of processing and analysis tools for time and frequency space analysis. The whole source code for IRlab is freely available for the research community under the General public license.

Conclusions: IRlab is a versatile tool for dynamic thermal image and video processing. Freeware and open-source programs for medical thermal imaging are severely lacking, thus as a completely open-source project IRlab offers a unique platform for researchers within the field of medical thermal imaging.

1. Introduction

Human body produces heat mainly through metabolic processes and muscle contraction, and the heat is transferred from the heart around the body through blood flow [1,2]. In an environment with controlled ambient temperature and moisture, and with minimal air flow the main contribution to the skin's thermal variations can be considered to originate from the blood perfusion [3]. Number of physiological factors affect the proper blood perfusion in the peripheral body parts, from which the lower limbs are at higher risk of complications due to primary diseases such as diabetes mellitus. Lower limb blood perfusion, i.e., the delivery of oxygenated blood and nutrients to the tissues can be permanently disturbed due to certain medical conditions, the most important of which is peripheral arterial disease (PAD) caused by atherosclerotic narrowing in the arterial tree. In the United States alone, there are over 12 million patients suffering from PAD [4]. Suitability of thermal imaging in the measurement of peripheral lower limb perfusion has been researched in numerous studies, especially with diabetes patients [1,2,5,6], and efforts to conceptualize the complex vascular networks entailing the blood flow within the lower limbs have been implemented with models, such as the concept of angiosomes, i.e. segments of tissue in which blood flow is covered by a single source artery [7–10]. The current clinical PAD diagnostic methods include physiological measurements, such as ankle-brachial index, toe brachial index transcutaneous oximetry (TcSPO2), toe systolic pressure and skin perfusion pressure. All of these methods require patient contact and do not offer spatial information apart from a single measurement point. Novel imaging methods such as indigo carmine angiography, perfusion imaging and magnetic resonance imaging expose the patient either to ionizing radiation, are invasive, require contrast agents or have limited

* Corresponding author. Tampereen yliopisto, Korkeakoulunkatu 3, 33720, Tampere, Finland.
E-mail addresses: tomppa.pakarinen@tuni.fi (T. Pakarinen), niku.oksala@pshp.fi (N. Oksala), antti.vehkaoja@tuni.fi (A. Vehkaoja).

https://doi.org/10.1016/j.imu.2022.100940
Received 30 December 2021; Received in revised form 28 March 2022; Accepted 1 April 2022
Available online 7 April 2022

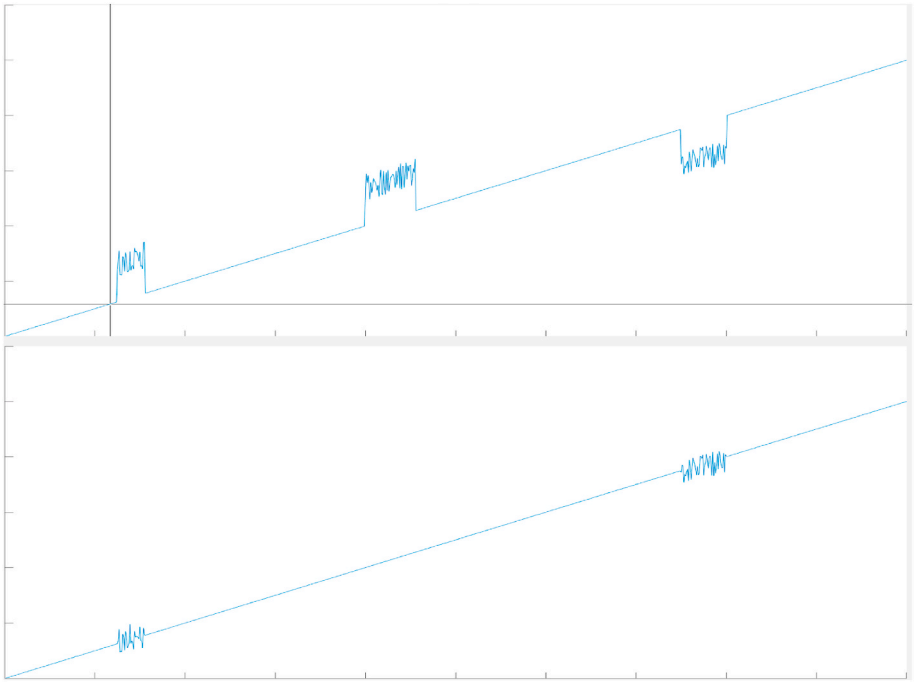

Fig. 1. Three artificial baseline artefacts on linear data corrected with recoverable, non-recoverable and offset methods, using linear interpolation.

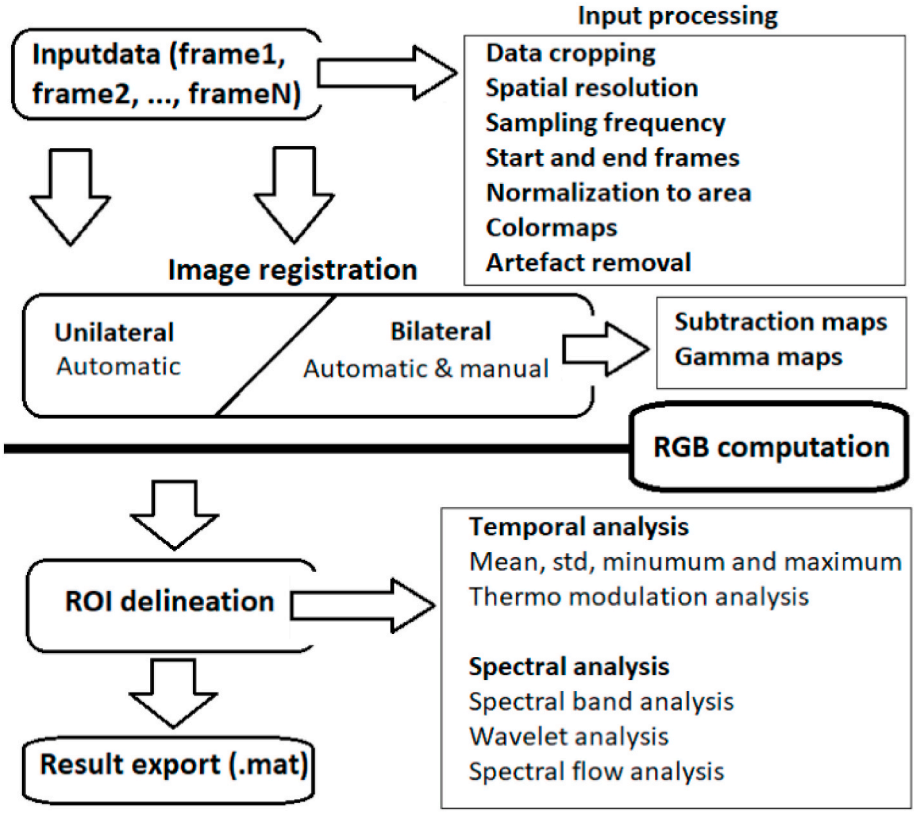

Fig. 2. IRlab workflow diagram. The workflow is divided by RGB computation in 2 main phases, indicated with a bolded horizontal line.

availability and the equipment is expensive. The substantial development of thermal imaging technology during the last decades offers multiple potential advantages over traditional thermal measurement methods and provides an interesting measurement modality for remote observation of body processes, especially due to its high spatial resolution and increasing sensitivity to small thermal variations.

In recent years, several groups have also studied the potential advantages in dynamic thermal imaging instead of the traditional steady state measurements. Dynamic approaches include active skin cooling and recovery response [11,12], power spectral analysis of temperature

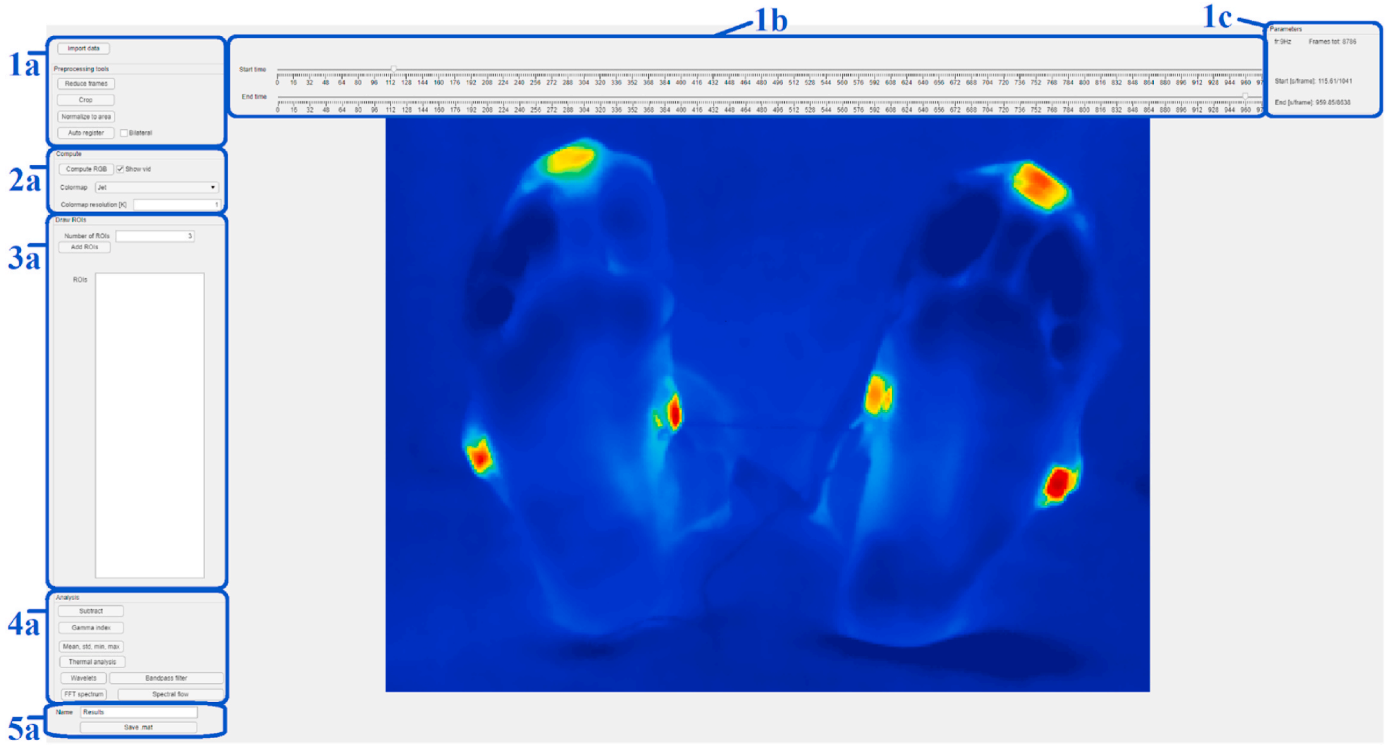

Fig. 3. IRlab user interface presenting labeled UI tool panels. The UI figure presents a test data set from the right (left side) and left (right side) lower limb. The hotspots seen in the image are optional thermal registration markers, attached to the lower limbs with an insulating layer between the marker and the limb.

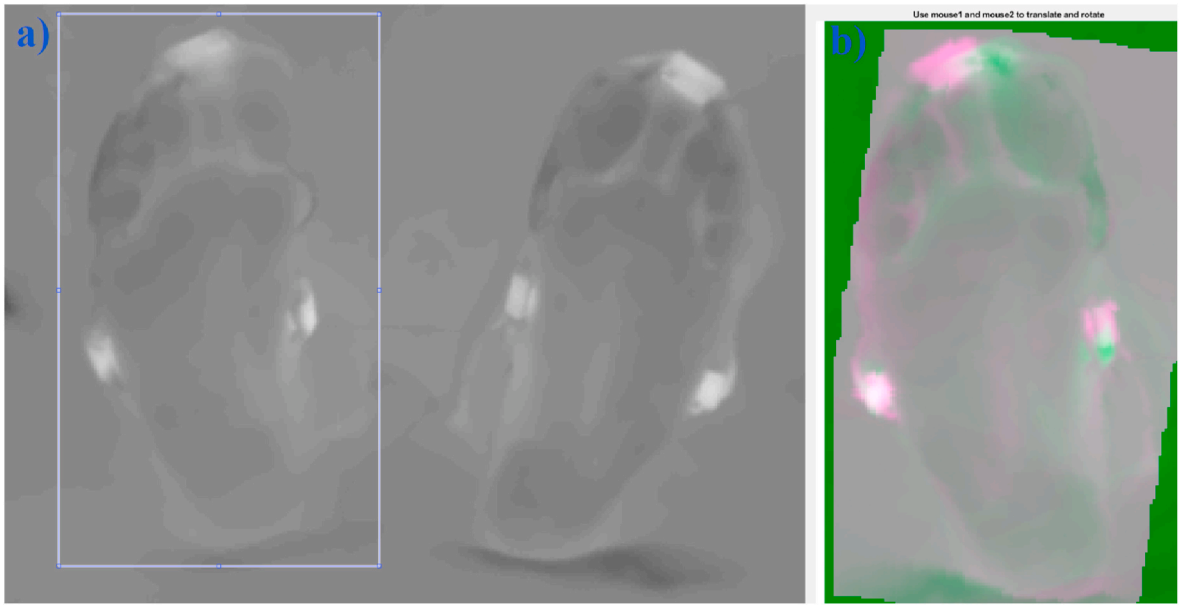

Fig. 4. Registration of ROI. Registration area is selected in subfigure a). The selection view is the same for uni- and bilateral cases, but in bilateral cases both sides (reference and target) are cropped successively. Subfigure b) presents the bilateral registration's manual phase, where the reference image (1st ROI) is registered with the mirrored target image (2nd ROI). Manual registration is performed for the reference images after the automatic bilateral video registration phase.

oscillations [13,14], reconstruction of blood flow from thermal variations [3], wavelet analysis of skin temperature variations [15], and spatial and temporal variations of thermal profiles [16]. Number of groups have also focused on thermal video processing methods, such as thermal motion tracking [17]. Also, thermal image registration is covered between thermal- and visible image registration [11,18,19], yet only few papers consider solely thermal image registration in the biomedical or medical field [16,20,21]. Other published computational methods for dynamic thermal analysis are spectral filtering methods [3,13,14], thermal oscillations [21], classification of vascular beds [16] and thermal modulation for active cooling [12,22,23]. However, analysis for the latter is mainly based on individual thermal images or on another sensor type rather than on thermal video or image sequences. The computation methods are usually presented sufficiently and Sagaidachnyi et al. share their blood perfusion converter tool as a free to use software but unfortunately, as far as we know, there are no other

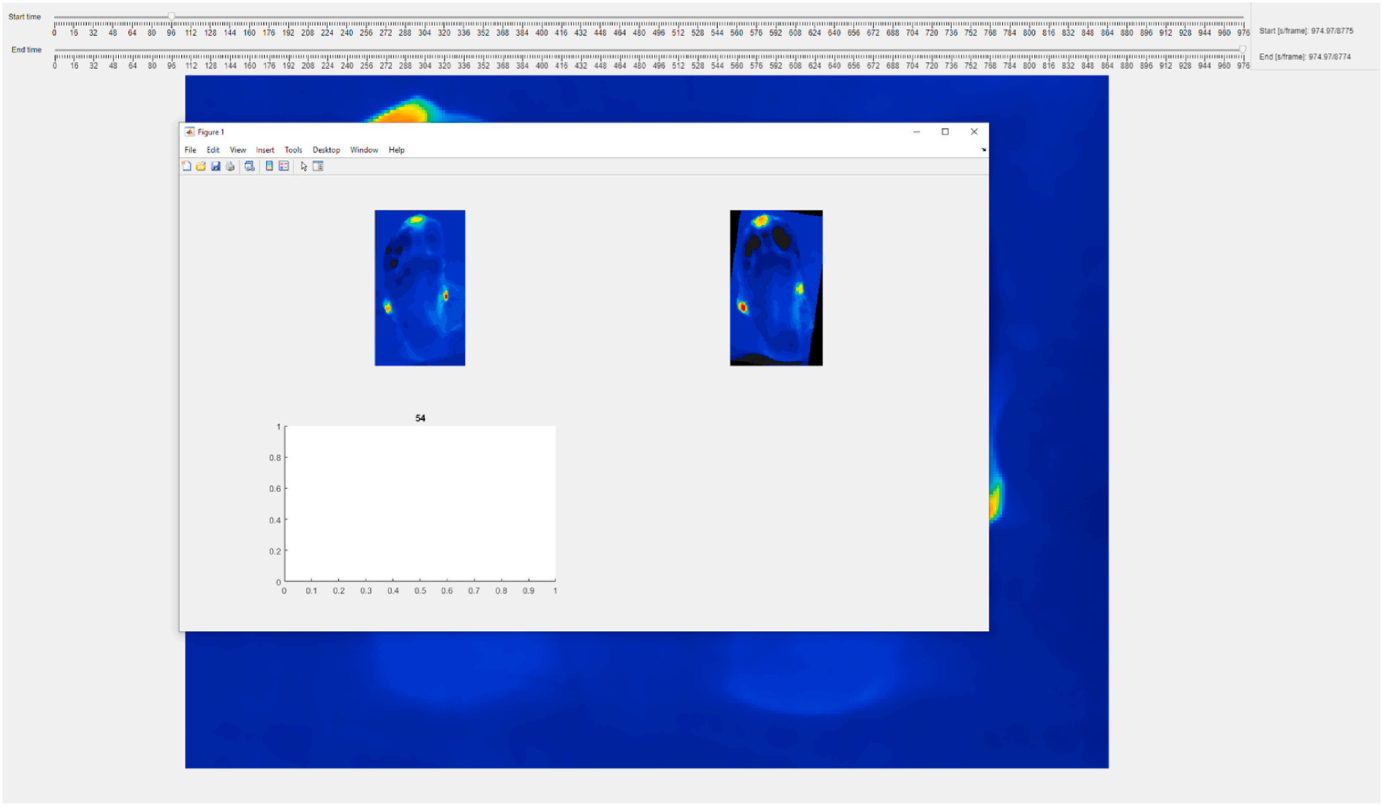

Fig. 5. RGB stack computation and registration success inspection.

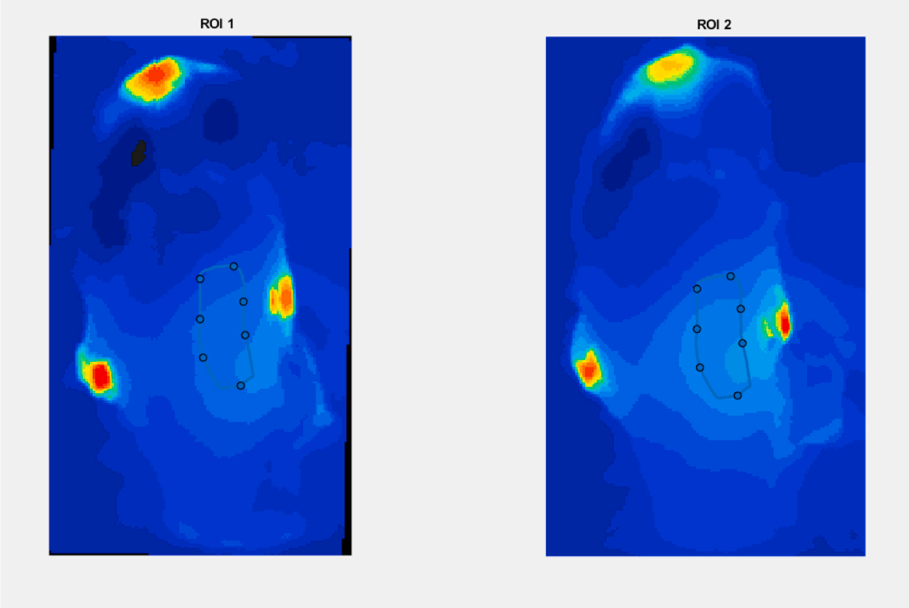

Fig. 6. Example from the angiosome drawing tool for a bilateral case. The first ROI is delineated on the reference image (ROI 1), which is then projected to the registered target image (ROI 2). Both ROIs can be modified separately after initial delineation. The three hot spots in both images are thermal markers attached to the lower limb to help image registration.

published freeware nor open-source programs or computational tools available. Thus, each group must either rebuild or purchase the analysis environment. The commercial software from the major thermal camera manufacturer's focus on thermal data acquisition and conventional viewing and graphing tools, rather than in depth analysis. Additionally, the current methods typically consider single images or steady state measurements. Hence, thermal imaging software supporting dynamic physical modulation tests has not been conducted.

IRlab aims to help researchers in medical thermal imaging by providing open-source tools with an easy-to-use user interface for dynamic peripheral thermal video analysis, especially aimed for lower limb perfusion analysis. IRlab combines multiple aforementioned

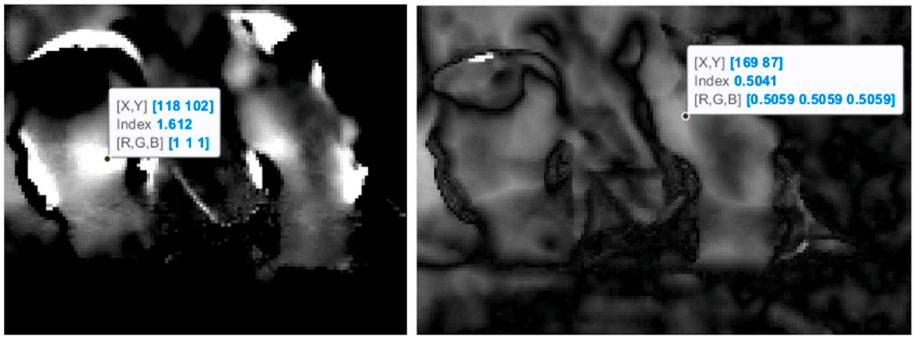

Fig. 7. Gamma (left) and subtraction maps between initial and end of recovery phases during cold provocation. Gamma indices over 2 units exceed the threshold for significant difference. Subtraction map presents the absolute temperature differences.

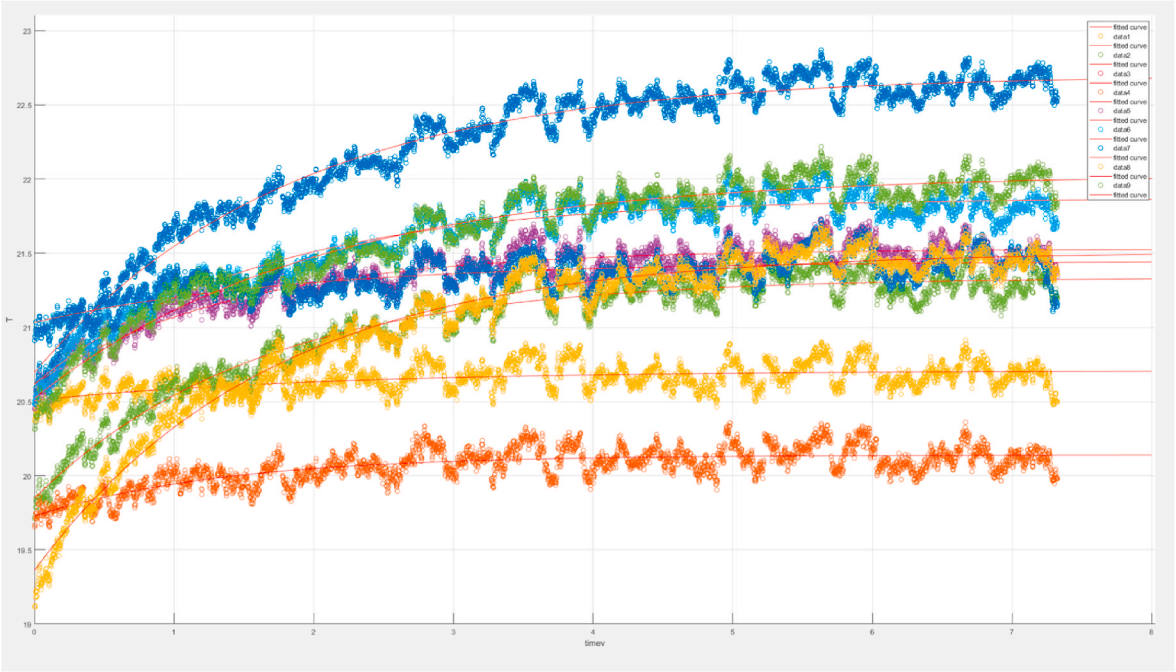

Fig. 8. Curve fitting using Eqn 4 for each measured angiosome.

methods under a single platform and further extends the analysis by several experimental methods. The proposed software focuses on lower limb analysis due to the nature and location of PAD manifestation and its most severe complication, critical limb threatening ischemia (CLTI). IRlab is free-to-use and offers the complete source code under the General Public Licence (GPL) 3.

2. Methods

IRlab is programmed completely with Matlab R2020a, v. 9.8 (MathWorks Inc., MA) [24]. The user interface is developed using the Matlab App designer environment. IRlab utilizes Matlab image processing and signal analysis toolboxes. Most relevant software properties and computational methods in IRlab are presented below.

2.1. Data import

The latest version (v. 1.0) supports comma-separated values (.csv) and Matlab (.mat) extension files for import. Import is performed by reading either parsed.csv files or the user can import.mat structures with required fields, i.e. structure consisting of each frame as 2D matrix as a field named 'frameN', where N is the frame index. All import data is expected to contain temperature values. The limited import alternatives originate from the lack of standardization for thermal image and video output files, thus each supplier has developed their own proprietary file formats. To import thermal video data directly from device to IRlab, the user must acquire manufacturer specific import files to be bundled with the software. The direct import may also require other manufacturer specific resources, which are often available only after purchase.

2.2. Temporal and spatial resampling and filtering

Typical modern thermal camera sampling rate ranges between 5 Hz and 30 Hz and for high-end high-speed cameras up to 10^5 frames per second [3], yet such high sampling rates are not often required. Thermal variations of the skin are slow and for example the frequency power spectral analysis and spectral filtering methods of human skin consider frequencies between 0.005 and 2 Hz [13], for which microbolometer cameras with noise equivalent temperature difference of 20 mK can extract information from only lower than 0.15 Hz bands, due to low SNR on higher frequency bands when considering the amplitudes of human skin thermal variations. Additionally, 98% of the spectral power lay within the 0.001–0.15 Hz band [14]. Thus, Nyquist sampling rate for thermal cameras with 20 mK NETD is about 0.3 Hz. In the test run

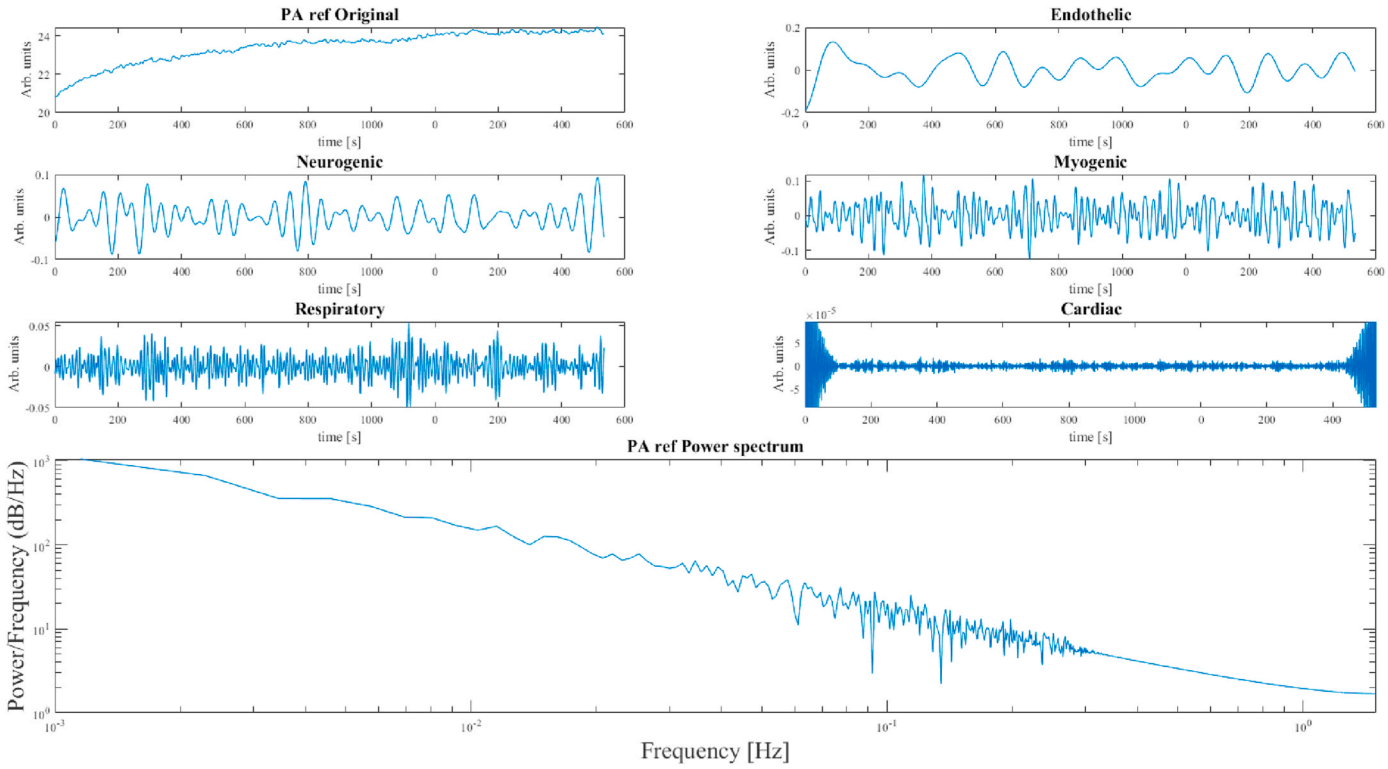

Fig. 9. Band pass filtered plots and power spectrums for unilateral plantar PA angiosome.

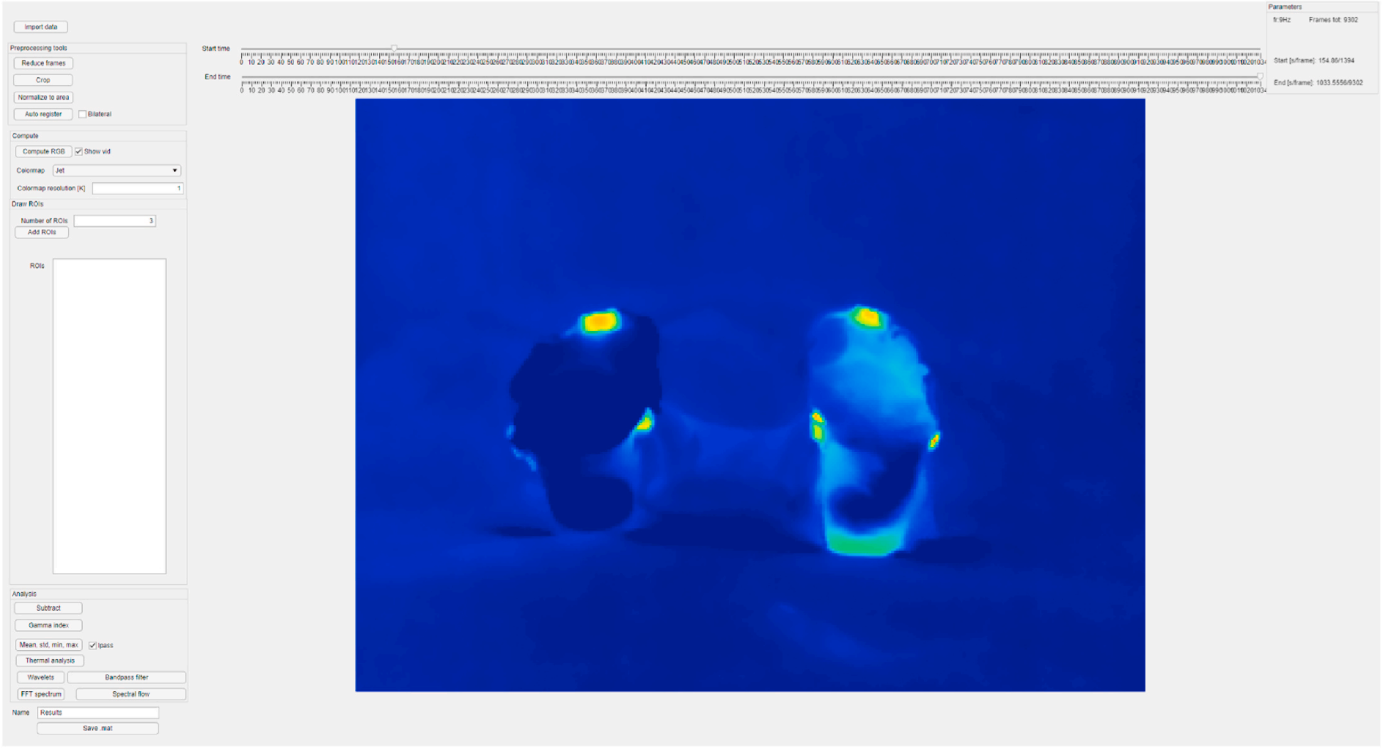

Fig. 10. Starting point right after the cold provocation. The right limb (reference) shows lower overall temperatures and less spatial thermal variability in comparison to the left limb (target). The hotspots around the limbs are thermal markers to aid in image registration.

presented in this study, the initial camera-sampling rate was reduced from 9Hz to 3Hz by averaging the excess frames with IRlab's frame averaging tool, after verifying that no significant limb movement takes place in this averaging period. Averaging decreases the required data registration time and increases temporal signal to noise ratio (SNR) with theoretical maximum factor of $\sqrt{n}$, where n is the number of averaging rounds, though the method is not effective in reducing the prominent $1/f$ noise in microbolometer cameras [26]. To speed up the processing and

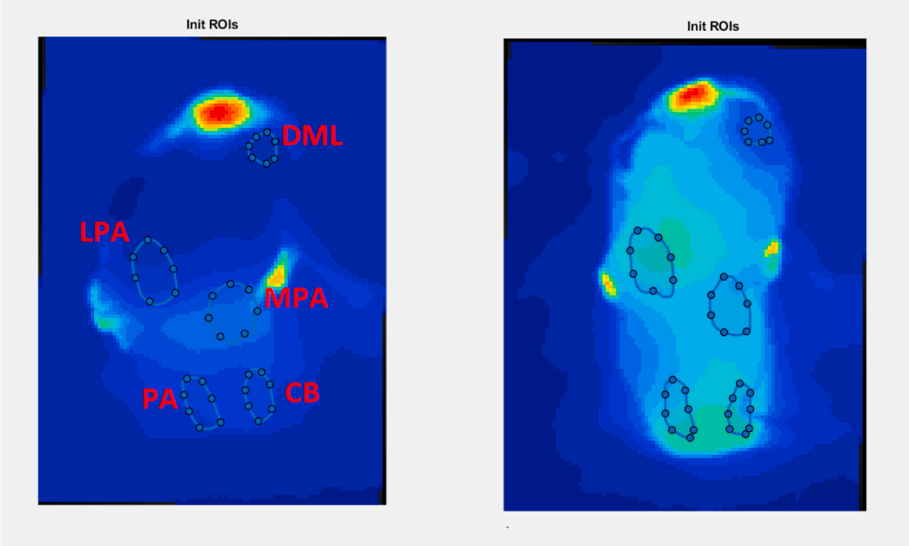

Fig. 11. Angiosome ROIs superimposed on the reference and target limbs on the initial frames before the cold modulation. The angiosomes are labeled on the reference limb.

analysis, and to increase spatial SNR, it is beneficial to lower the spatial resolution from high-resolution cameras by using a spatial median filtering or averaging the neighborhood pixels. Median filtering is usually sufficient when there are no small targets of interest [25]. This method also requires that there are no significant temperature gradients within the neighborhood scale and high-resolution images are not required for any other reason. Our initial testing concluded that 320x240-pixel resolution is sufficient to analyze both lower limbs simultaneously, when confined properly within the imaging area.

2.3. Image registration

Object motion correction has an essential role in dynamic thermal imaging, since involuntary movement and drifting cannot usually be avoided. Physical motion prevention would require e.g. body part fixation, which is not reasonable for long periods of time or in dynamic modulation tests. IRlab allows the user to perform unilateral image registration for a single rectangular region of interest (ROI), intended to contain a single body part. Alternatively, the user may perform bilateral registration of two symmetrically positioned body parts, such as lower limbs. In a unilateral case, the image registration is performed using a single rectangular ROI over all frames against a chosen reference image, i.e. the first frame within the analysis period. The registration uses mono- or multimodal intensity-based image registration with a variable number of iteration rounds, i.e., the image resolution is changed iteratively until the optimization process converges or the maximum number of iteration rounds is reached. Multimodal option may be needed if the imaged thermal profile changes considerably over the imaging period, e.g., during active cooling modulation. Automatic registration properties may also be changed from rigid to affine. IRlab utilizes Matlab's image processing toolbox for intensity-based image registration [24].

For bilateral cases, first two rectangular ROIs are cropped from a reference image, consisting of bilateral body parts, e.g., left and right lower limb and both ROIs are registered first independently against their respective cropped reference frames. After the automatic registration phase, the user performs manual rigid registration between the reference side (e.g., right limb) and the mirrored target side (left limb). Translation and rotation vectors are saved from the manual registration and used to operate the prior, automatically registered target video data, resulting in a bilaterally registered dataset.

2.4. Gamma index and subtraction maps

Gamma index is a robust method to measure local similarity between two datasets. Instead of measuring pixel-by-pixel absolute temperature differences, the gamma index also considers high gradient areas, where small spatial shifts in data may produce a large error to the absolute difference. The gamma index computation is performed for each data point by minimizing the squared sum of the gamma components, i.e. distance to agreement (DTA) and temperature difference (TD), relative to their respective gamma criteria. Gamma indices are calculated as presented in Eqn 1

$$\gamma(r_m) = min\{\Gamma(r_r,\ r_t)\}\ \forall\{r_r\} \tag{1}$$

where r_r and r_t refer to the reference and target spatial locations and where

$$\Gamma(r_r,\ r_t) = \sqrt{\frac{|r_r - r_t|^2}{\Delta d_r^2} + \frac{|T_r(r_r) - T_t(r_r)|^2}{\Delta T_r^2}} \tag{2}$$

In Eqn 2, $|T_r(r_r) - T_r(r_r)|^2$ is the squared difference between target and reference temperatures, and Δd_m and ΔT_m are the DTA and TD criteria, respectively [27]. Gamma computation has been originally developed for dosimetry evaluation in radiotherapy, thus the DTA and percentage difference criteria cannot be directly used in thermal evaluation. The user must define the criteria, and their value depends on the characteristic temperature differences and temperature gradients for the inspected object. Weighting too much of any of the components can lead to exaggeration of the gamma indices at isotropic areas (too high DTA weight) or at high gradient areas (too high TD weight). IRlab utilizes an open source CalcGamma function for gamma indices computation [28]. We suggest a possible advantage of gamma map over the temperature difference alone, for its ability to weight temperature gradients, which could be useful e.g. in hotspot detection and delineation.

Since using gamma indices outside of radiotherapy is unconventional, IRlab is using subtraction map computation as the default analysis method. Subtraction maps are computed as in Eqn 3 by simply taking the latter squared part from the Eqn 2

$$T_{diff} = T_r(r_r) - T_t(r_r) \tag{3}$$

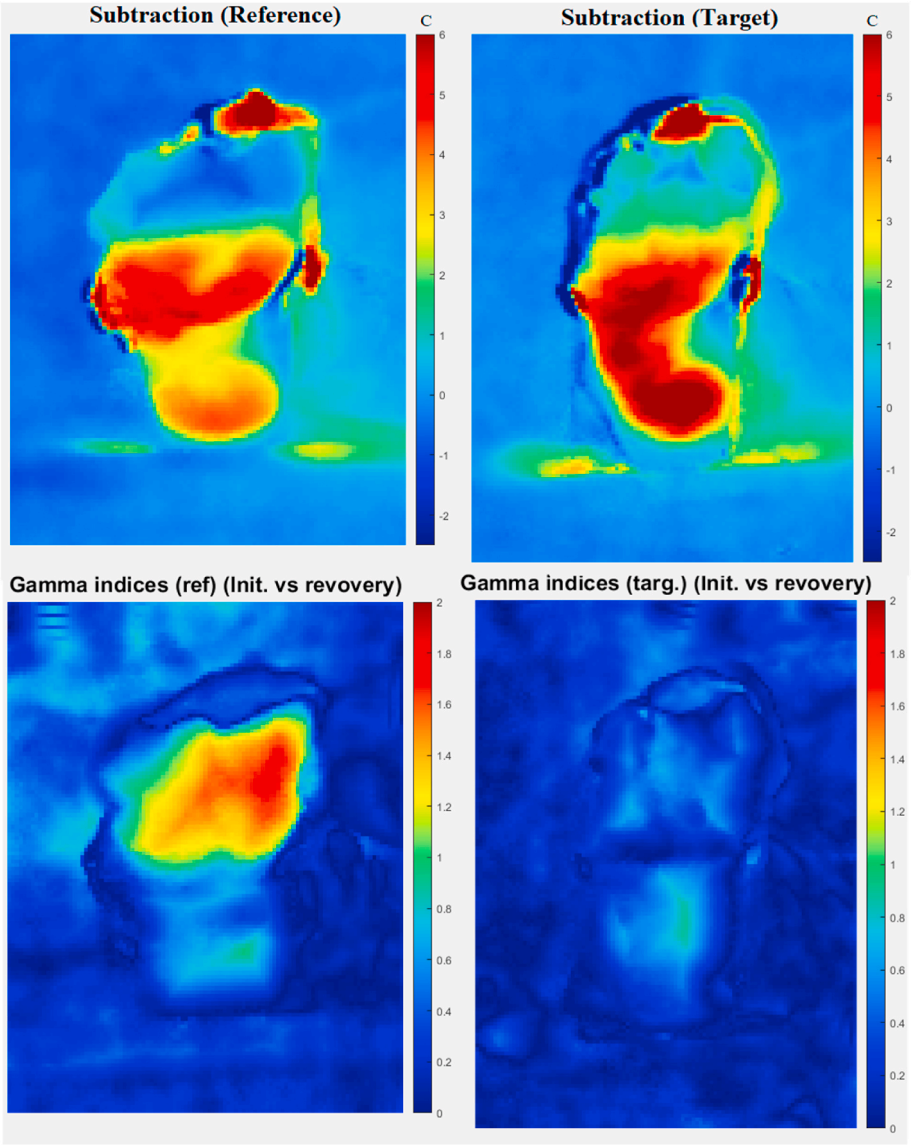

Fig. 12. Subtraction maps (top row) at the start and end of the cold provocation and gamma indices (bottom row) between the end of the recovery period and the initial temperatures prior to the cold provocation. Visual inspection of both maps shows signs of reduced recovery flow within the DML angiosome, and partly in the LPA and MPA angiosomes of the reference limb.

2.5. Region of interest delineation and bilateral projection

ROI drawing tool utilizes polygonal freehand drawing functions for interactive angiosome delineation. The polygon vertices are used to compute binary masks for each delineated ROI. Additionally, the polygon centroids are computed and saved as the locations for neighborhood determination e.g. in spectral filtered flow computation (see section 2.9). If the bilateral option has been chosen, the reference ROI is delineated in the reference side and projected to the mirrored target side (see section 2.3). In case of imperfect registration or asymmetrical anatomy, both ROIs may be modified interactively after initial drawing. There is no limit for the total number of ROIs.

2.6. Thermo modulation analysis

Dynamic thermal modulation tool analyses thermal recovery, caused by active cooling or possibly the effects of active heating of an anatomical location. The analysis uses the median values, computed for each ROI to fit an exponential function, presented in Eqn 4.

$$T(t) = T_0 e^{(-t/\tau)} + A\tau\left(1 - e^{(-t/\tau)}\right) \quad (4)$$

where T_0 is the initial temperature after thermal provocation, A is a constant and τ is the thermal time constant. The exponential function fit can be evaluated with goodness-of-fit (GOF) parameters and by the visual shape of the recovery curve. Finally, time constant τ Eqn 4 is solved and saved to the respective ROI structure together with the GOF-parameters. We hypothesize that normal, unrestricted, and healthy perfusion to a single artery sourced angiosome [29] follows during thermal recovery, with a time constant proportional to the vascularization and perfusion of the area. Perfusion in angiosomes covered with several source arteries could possibly be modeled as the superposition of the source arteries proportional contribution.

2.7. Artefact removal

IRlab includes an artefact removal tool [30] for computed 1D temperature curves, which can be used in three types of artefacts from the extracted median curves for each ROI. The removal methods are

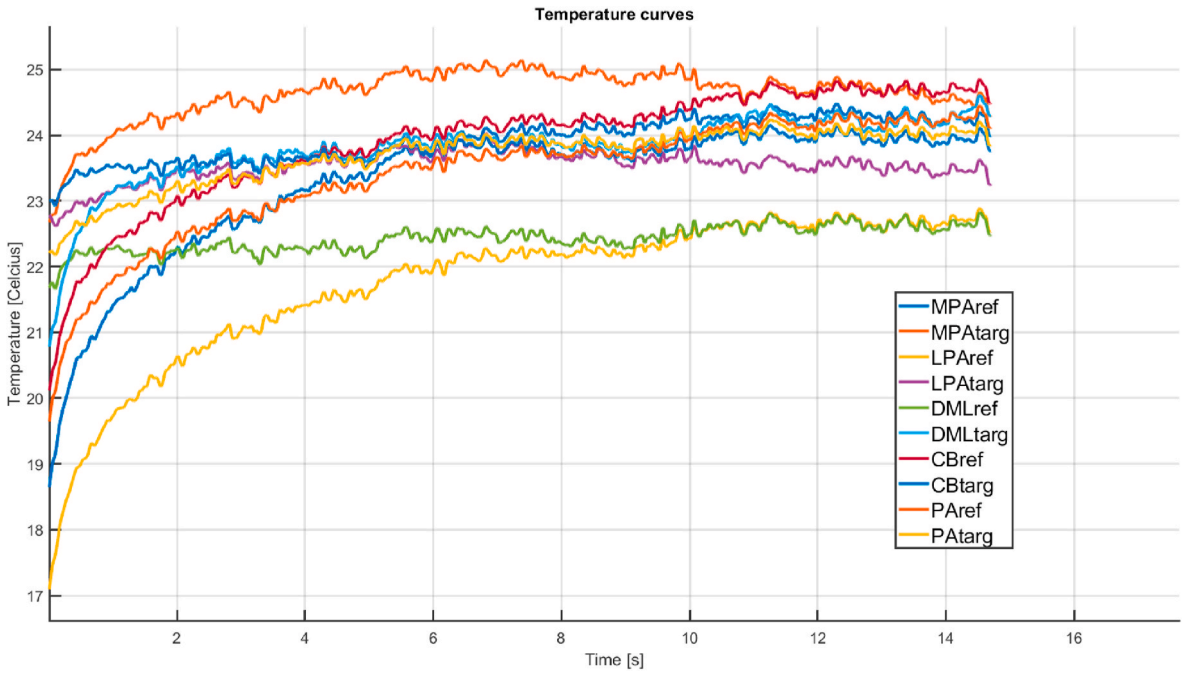

Fig. 13. Median temperature curves of each angiosome.

	1 MPA_ref	2 MPA_targ	3 LPA_ref	4 LPA_targ	5 DML_ref	6 DML_targ	7 CB_ref	8 CB_targ	9 PA_ref	10 PA_targ
1 timeconstant	3.1692	5.1737	2.9571	3.4199	69.0256	17.7878	2.8043	14.0460	3.0339	3.1815
2 Tstart	20.9882	23.6396	18.8901	22.8597	22.4073	23.3737	21.7773	23.5710	21.2882	23.5447
3 Tend	24.3805	24.1175	22.6401	24.6275	23.2093	23.6631	24.6434	23.8267	24.2771	25.3578
4 Tend-Tstart	3.3924	0.4779	3.7500	1.7678	0.8020	0.2894	2.8661	0.2557	2.9889	1.8132
5 Tstart-T0	-5.2236	0.9308	-5.4347	-2.4065	-1.6409	0.5310	-4.6857	0.7375	-4.8949	-2.9634
6 Tend-T0	-1.3860	1.6101	-1.2893	-0.4207	-0.8144	0.9803	-1.4338	1.1136	-1.6380	-0.8766

Fig. 14. Results from cold provocation test analysis. Column names refer to the angiosomes and row names to the test parameters, where T0 is the temperature prior to the cold provocation, Tstart is the temperature after the provocation and Tend is the temperature at the end of the recovery.

	1 MPA_ref	2 MPA_targ	3 LPA_ref	4 LPA_targ	5 DML_ref	6 DML_targ	7 CB_ref	8 CB_targ	9 PA_ref	10 PA_targ
1 sse	43.5968	23.5759	41.4146	26.6892	39.6873	22.3047	34.8605	21.5530	33.9355	29.0213
2 rsquare	0.9873	0.6294	0.9875	0.9722	0.4496	0.5548	0.9806	0.5320	0.9827	0.9678
3 dfe	3897	3897	3897	3897	3897	3897	3897	3897	3897	3897
4 adjrsquare	0.9873	0.6292	0.9875	0.9721	0.4493	0.5546	0.9806	0.5318	0.9827	0.9678
5 rmse	0.1058	0.0778	0.1031	0.0828	0.1009	0.0757	0.0946	0.0744	0.0933	0.0863

Fig. 15. Goodnes-of-fit (GOF) evaluation results for the exponential function fit. The validity of the results in the cold provocation test analysis should be reconsidered if the GOF parameters indicate a poor exponential fit.

manual, i.e. the user selects manually the artefact locations. For the cases where data has a corrupted section, which is not recoverable, the data is interpolated from selected starting point to the end point via linear interpolation. For recoverable data, i.e., baseline or low frequency artefact, the user may choose either data offset value or high pass component injection. Data offset method simply offsets the chosen region by a chosen value. The component injection first extracts a high pass filtered component from the chosen region, then interpolates the section as in the non-recoverable method interpolation, and finally superimposes the high pass filtered component to the interpolated region.

The used artefact removal methods are presented in Fig. 1. The recoverable method preserves the high frequency signal features e.g., in cases of non-uniformity correction (NUC) baseline shifts. However, the user should always consider if such baseline correction is required.

2.8. Spectral analysis

Spectral analysis operates the input ROI median values with a minimum order infinite impulse response bandpass filter using 60 dB stopband attenuation. To suppress the transient filter response artefact, 1000-point data padding is added prior to the filtering and truncated from the filtered signal. IRlab supports 0.005–0.02 Hz, 0.02–0.05 Hz, 0.05–0.15 Hz, 0.15–0.4 Hz, and 0.4–2.0 Hz band filtering, which correspond to endothelial, neurogenic, myogenic, respiratory, and

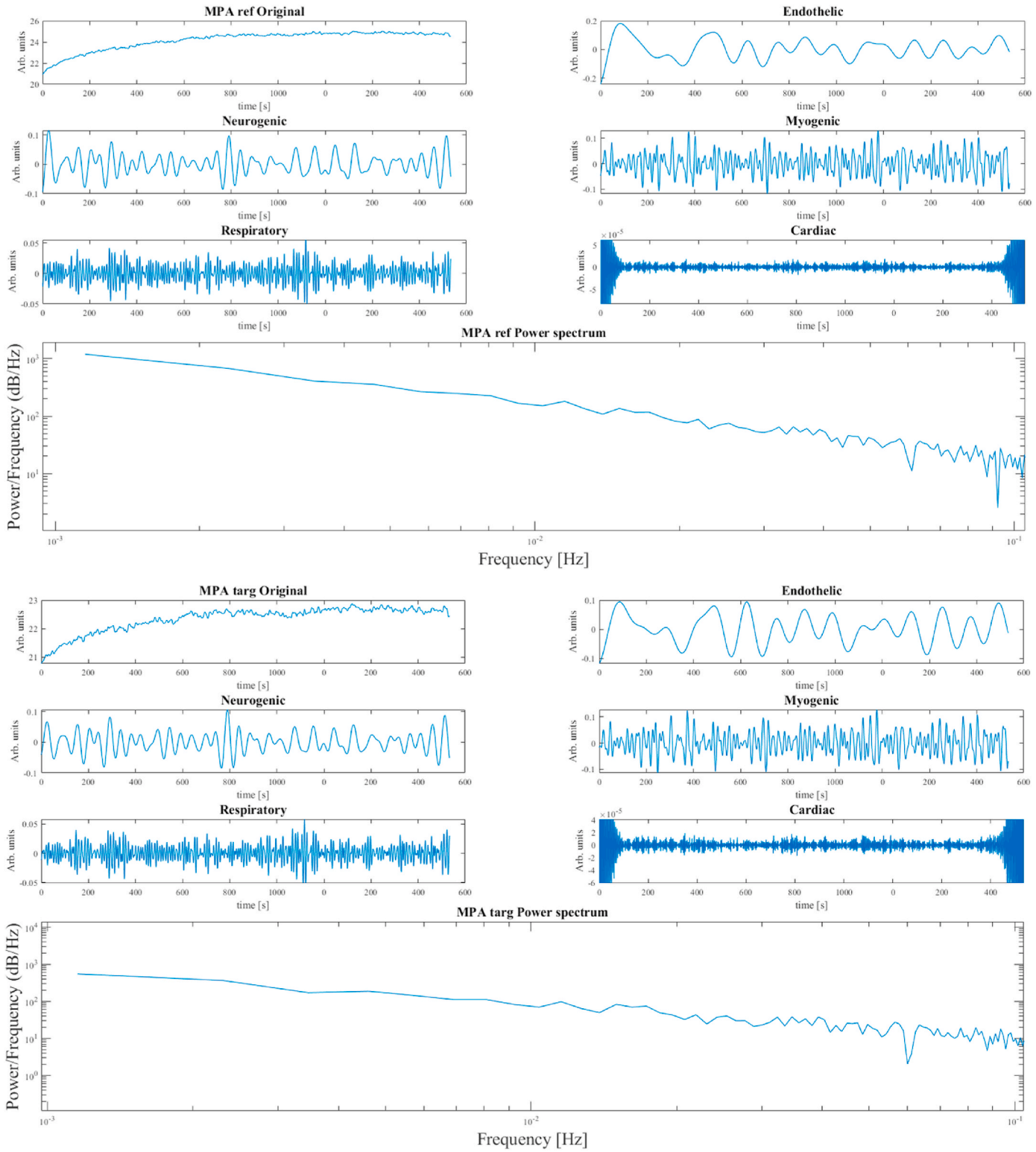

Fig. 16. Spectral bands (endothelial, neurogenic, myogenic, respiratory and cardiac) of the MPA angiosome for both reference (above) and target (below) limbs. Note the respiratory, cardiac and major part of the myogenic bands cannot be used due to low SNR resulting from high camera NETD.

cardiac origins, respectively [3,13]. The reduction in each band power has been previously connected to the change in perfusion from the above-mentioned sources, but useful information is mainly concentrated within the 0.005–0.15 Hz range. With current thermal cameras, the respiratory and cardiac band SNR remains too low for extracting any useful information [3]. Thus, an additional bandpass filter with 0.001–0.2 Hz frequency range is suggested for NEDT values higher than 20 mK. Spectral analysis tool computes the power spectrum and the band power for each ROI. The power spectrum analysis is mainly intended for steady state measurements since FFT loses the temporal frequency information, thus neglecting the time dependent dynamic component e.g., in thermal modulation test. In cases of non-steady state measurement, the user may additionally use the wavelet analysis tool, which computes the continuous wavelet transforms and scale-to-period

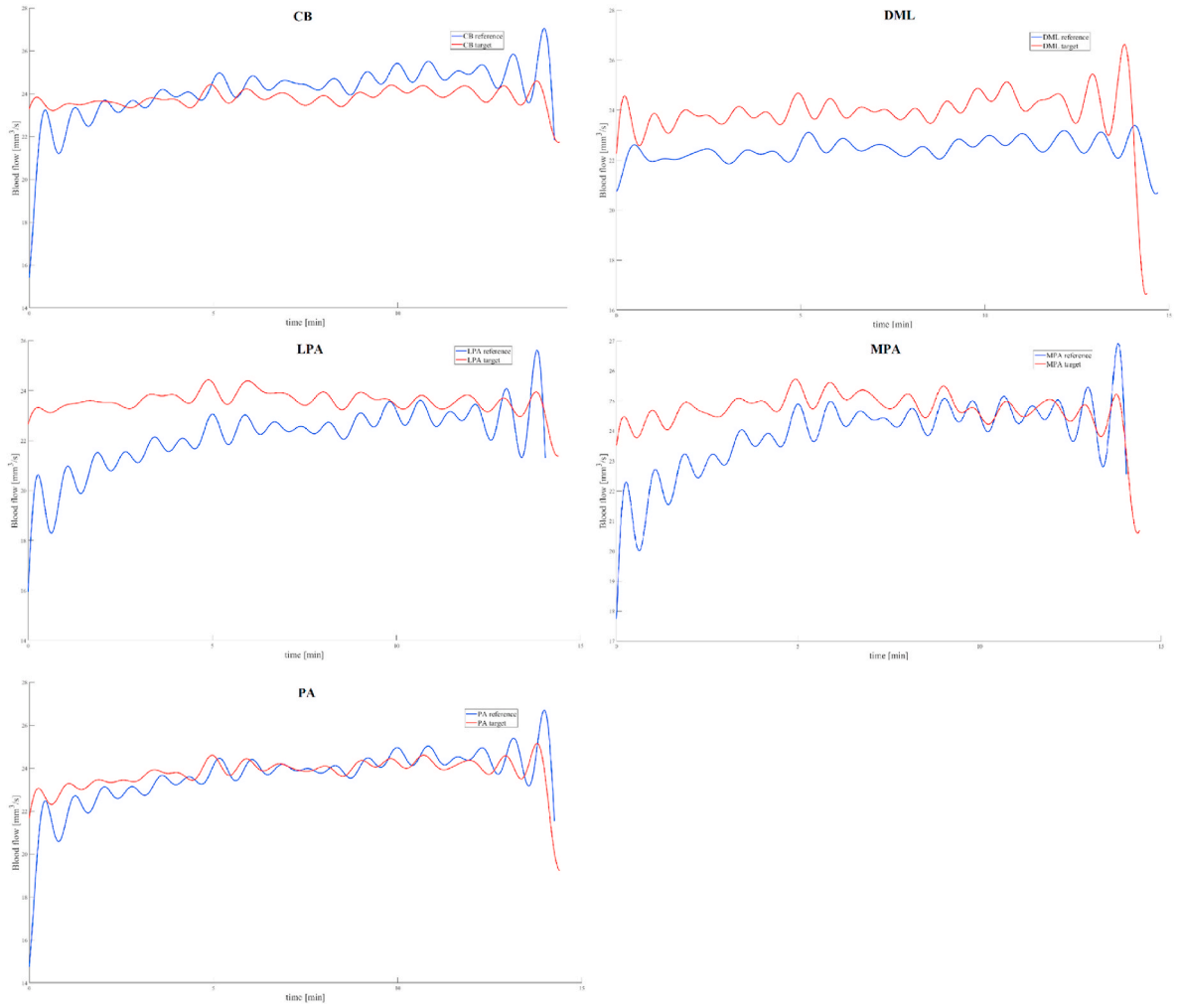

Fig. 17. Endothelial blood flow (0.02 Hz) level estimation curves from each angiosome's median values. Blue curve presents the reference (right limb) limb's angiosomes and the red curve the target's (left limb). The plots indicate relative decrease of flow within the reference DML angiosome and slight decrease in the LPA and MPA angiosomes, in agreement with Fig. 12. (For interpretation of the references to color in this figure legend, the reader is referred to the Web version of this article.)

conversions, using the Morlet-wavelet as the default convolution kernel.

2.9. Spectral filtered temperature to blood flow reconstruction

Bloodflow $S_{BF}(t)$ reconstruction from thermal signal $S_T(t)$ is based on the spectral filtering of the endothelial, neurogenic and myogenic frequency bands as described by Sagaidachnyi et al. [3]. The IRlab implementation computes Fast Fourier Transform (FFT) to transform the whole polygonal ROI area and computes the flow plots for center of mass pixels along the image stack time dimension with a spatial average from 1 pixel radius neighborhood. The FFT of the convolution kernel is an exponential amplitude - phase modulation function operating on $S_T(f)$, i.e. $F\{S_T(t)\}$, *s.t.*

$$S_{BF}(f) = exp\left(z\sqrt{\frac{\pi f(c\cdot\rho)}{k}}(1+i)\right)\cdot S_T(f), \tag{5}$$

where $S_{BF}(f)$ is $F\{S_{BF}(t)\}$, k is the heat conductivity of the skin, c is the specific heat capacity of the skin, ρ is the skin density and z is the skin thickness and f is the frequency. The convolution between $S_T(t)$ and the kernel modulates the frequency specific amplitude absorption and phase delay, resulting in an estimation of total blood flow. Eqn 6 represents the amplitude modulation part from Eqn 5

$$exp\left(z\sqrt{\frac{\pi f(c\cdot\rho)}{k}}\right) \tag{6}$$

and describes the depth dependent absorption rates of different thermal oscillation frequencies, and the Eqn 7 phase delay

$$exp\left(iz\sqrt{\frac{\pi f(c\cdot\rho)}{k}}\right) \tag{7}$$

which considers the transmission delay for these oscillations [3]. The final time dependent blood flow is obtained via inverse Fourier transform, i.e. $S_t(t) = F^{-1}\{S_{BF}(f)\}$.

3. Results

3.1. Software workflow description

Workflow in IRlab can be divided roughly in two main phases, i.e., preprocessing phase and analysis phase, which are separated by RGB computation. RGB computation creates an RGB image stack, which is used for determining the ROI-areas and as visual reference to the original image data. The preprocessing phase consists of data import, preprocessing and image registration steps, after which the RGB stack is computed. The analysis phase is initiated with ROI delineation from the

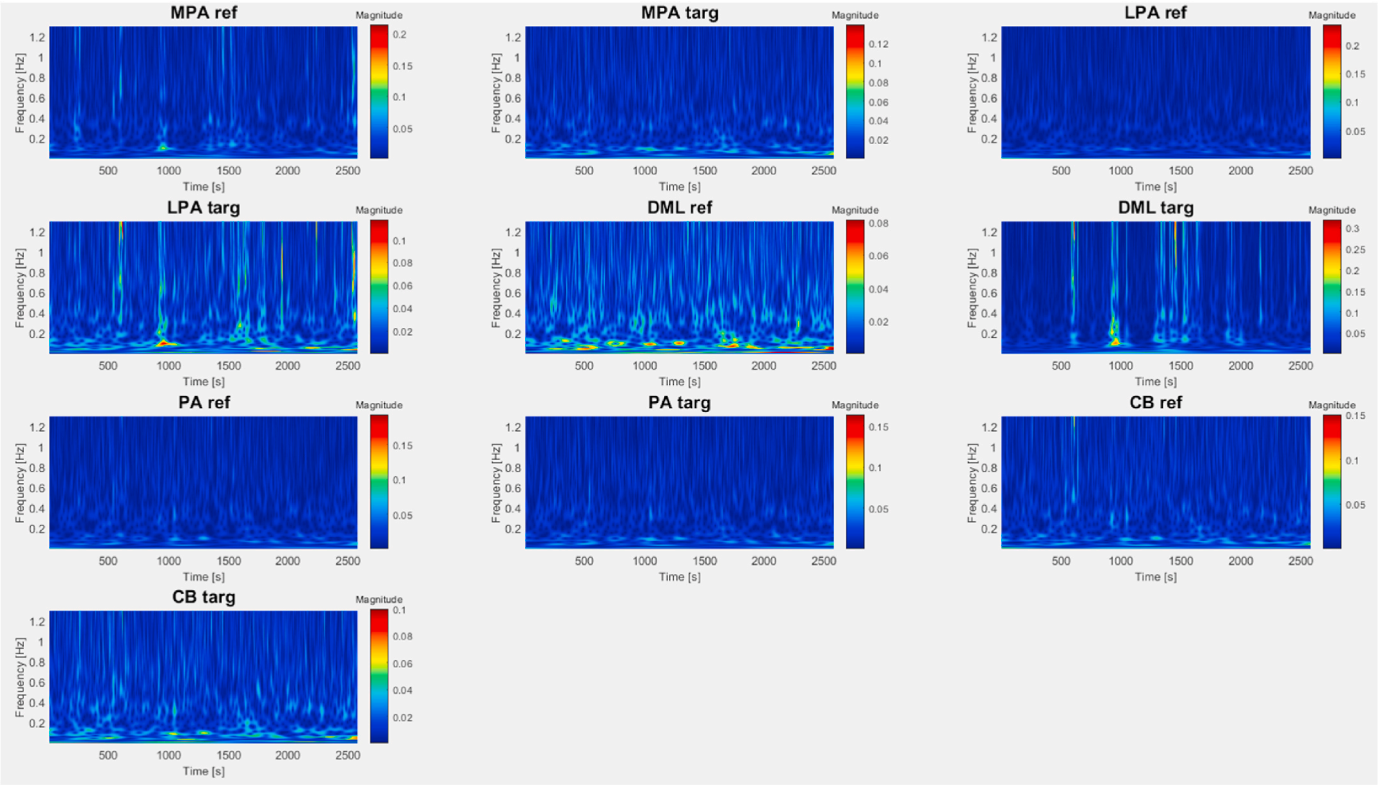

Fig. 18. Wavelet magnitude scalo-grams for each angiosome.

RGB images and followed by time and frequency-based analysis steps. The complete workflow is shown in Fig. 2.

After RGB computation is performed and if the user wishes to change the input processing parameters, the RGB must be recomputed. Recomputation of a given analysis after modifying preprocessing parameters will replace any prior computation results for the step. Otherwise, the results of previous instances are preserved until overwritten. Final results are saved via.mat export.

3.2. *Program description*

IRlab is programmed completely with Matlab R2020a (v. 9.8), due Matlab's extensive usage within the scientific community and numerous inbuilt toolboxes and functions, which support data visualization and analytics. IRlab will be compatible with future Matlab versions since it has been created in the App Designer platform instead of graphical user interface development environment (GUIDE). The user interface (UI) is presented in Fig. 3

The user interface is divided in numbered subsections, which also indicate the workflow phase within the program. Section 1a) holds the import data button and preprocessing panel i.e., normalization to an object, re-sampling, and registration UI properties. Section 1b) contains the timeline sliders for the thermal video. In the first workflow step, the input data is imported via the import button, and the start and end sliders are used for analysis start and end point search. The UI main figure shows the video frame corresponding to the slider positions. Also, in section 1c), the program shows the camera frame rate and current frame and time in seconds. After the start and end time points are chosen, resampling may be used to reduce the analyzed frame rate with or without averaging. Next, the image data can be registered using the 'Auto register' button. The video registration has two options, which can be toggled using the 'Bilateral' checkbox located in UI group 1a). When checked, the program performs a bilateral analysis workflow. Otherwise, the analysis is performed unilaterally. The registration views are presented in Fig. 4.

UI group 2a) in Fig. 3 contains RGB image and temperature colormap computation. The user may compute the RGB images in the background or display an RGB video during transformation for registration result inspection. The UI presents the RGB as sped up video and temperature curve for a chosen sample point as presented in Fig. 5. Registration can be recomputed at any stage, if needed.

UI group 3a) contains the ROI/angiosome drawing tools and 2 checkboxes for bilateral analysis. If none are chosen, the ROIs are drawn for the reference i.e., the first registered data set. Otherwise, the target dataset is included in the analysis. The dual ROI checkbox dictates if the delineated ROI from the reference image is projected to the mirrored target image. If a 'bilateral' option is chosen but 'dual' ROI is not, no data mirroring is performed and the user must draw all ROIs manually (see Fig. 6).

Each ROI is named prior to the delineation and added to the 3d) listbox. Bilateral ROIs are labeled with 'ref' and 'targ' subscripts. ROIs can be activated from the listbox, after which they are visualized in the main UI figure window overlayed with the original image data. Sliders in UI group 1b) may be used to inspect the ROI positioning throughout the thermal video.

The subtraction and gamma analysis buttons in UI group 3a) can be used to compute a subtraction image or a gamma map between start and end frames of the analysis. Registered data is used automatically, when the frame registration phase is performed prior to the subtraction and gamma map computation. Otherwise, only the unregistered results are saved. Fig. 7 shows the unregistered greyscale results from subtraction and gamma computation.

UI group 4a) contains the thermal and spectral analysis tools. Analysis is only performed to the ROIs selected from the UI group's 3a) listbox. 'Median, sd, max, min' button computes the respective parameters, plots the results and saves them to a result structure. The thermal analysis button performs the thermal modulation analysis, including exponential function fitting, time constant determination and GOF-

parameter computation. Resulting curve fits are presented in a separate figure (see Fig. 8).

Bandpass filtering button computes the frequency band passed components for endothelial, neurogenic, myogenic, respiratory and cardiac bands together with ROI power spectrum as shown in Fig. 9.

The results are again presented in a set of separate figures and saved to the results structure. Finally, the spectral flow button reconstructs the ROI specific blood flow from the thermal data (see section 2). The results are saved to the results structure. UI group 5a) consist of a name field and a save button. The save button will store the results to a structure as. mat format for later processing and analysis.

3.3. Sample run

Sample run was performed using data from a cold provocation test for a single individual, with no history of vascular diseases, on the plantar side of the lower limbs. First, the data was imported to IRlab and the frame rate was reduced to 3 Hz by averaging. The start of the cold provocation period was scanned with the 'start time' slider using the default colormap and the 'end time' slider was set to the last datapoint (see Fig. 10). No other preprocessing was performed.

Next, a bilateral analysis workflow was chosen, and the dataset was registered using rigid transformations with 20 iteration rounds and a multimodal optimizer. Bilateral registration results were visually validated using the RGB video display option, while computing the RGB image stack. Next, 5 angiosomes: Medial plantar (MPA), Lateral plantar angiosome (LPA), Calcaneal branch (CB), Peroneal angiosome (PA) and hallux (DML) were delineated from the RGB reference image. Angiosome ROIs were drawn on the reference images, from which they were projected to the mirrored target image stack. Each ROI was also slightly modified after initial drawing to match the relative positions and size on both limbs (see Fig. 11).

Subtraction and gamma maps were computed and saved for the cropped image areas. Both maps are presented in Fig. 12.

Next, median, minimum, maximum and standard deviation values were computed for each angiosome. The temperature recovery curves are presented in Fig. 13.

Next, the thermal analysis was performed for the median angiosome values, using the exponential function (Eqn 4) fit and the heating parameters, i.e. goodness of fit and time constant, were evaluated (see Fig. 14 and 15).

Before any further analysis, median data was low pass filtered with >0.15 Hz stopband and 60 dB stopband attenuation to neglect data outside of the predefined bands (section 2.8). Band powers were computed for each angiosome within endothelial and neurogenic bands. Example angiosome (MPA) bands and band power for both limbs are presented in Fig. 16.

Additionally, bilateral thermal flow analysis was performed for each angiosome. The flow analysis (Eqn 5) was performed to the median angiosome temperatures and only for the endothelial frequency band in this sample run. To preserve the lower frequencies due to temperature modulation test, the data was filtered with an infinite impulse response filter with a stopband frequency set to 0.02 Hz. The skin parameters were set to $k = 0.33\ W/(m \cdot K)$, $c = 3780\ J/(kg \cdot K)$, $\rho = 1057\ kg/m^3$ and the effective skin thickness $d = 2\ mm$. The endothelial band blood flow estimations are presented in Fig. 17.

Finally, a wavelet analysis on each ROI was computed using Morlet-wavelet as the convolution kernel. Scale-to-frequencies conversions were saved for visual inspection. The resulting magnitude scale grams are presented in Fig. 18.

4. Discussion

IRlab provides a variety of processing and analysis options for time and frequency based dynamic thermal analysis. IRlab also offers a clear workflow which can be combined with thermal modulation tests. Bilateral delineation of multiple ROIs allows perfusion area division based on the angiosome concept, which has a variety of possibilities in the modern lower limb peripheral artery disease diagnostics [7–10]. In addition, novel computational methods such as blood flow reconstruction from slow temperature variations may constitute a better estimation of the real peripheral perfusion, especially when combined with the other thermal metrics. IRlab is developed principally for lower limb thermal analysis, based on the angiosome concept, though there are no limitations for its use e.g. for upper body peripherals. IRlab is an ongoing open-source project and is under constant development. This means that the program, the methods used in the program and their validation has several known and unknown limitations and require further testing and research. For example, Sagaidachnyi et al. concluded that 98% of the spectral power and thus the majority of the information in temperature variations lay within endothelial, neurogenic and myogenic bands, and that camera sensor's NETD should be 20 mK at maximum to have sufficient signal to noise ratio within all three bands [3]. Unfortunately, our test equipment (FLIR E8) has NETD of 60 mK, which is not sufficient to extract information from frequencies above the neurogenic band, i.e. cardiac, respiratory and myogenic band information is lost. Other limitations due to the test equipment performance relates to the power spectral and wavelet analysis, which will be further tested in our future research using high end thermal cameras, with 10–20 mK NETD, high sampling rates and spatial resolution. Additionally, since dynamic thermal video analysis in the medical field is not yet well established, thermal image registration requires optimization and is currently time consuming, unrobust and may require thermal markers especially if the target body part temperature overlaps with the background.

5. Conclusions

Dynamic thermal imaging is a promising method for peripheral vascular diagnostics. Dynamic modulation and thermal video extends the standard thermal imaging, which is based on individual images, thus providing no information about time dependent hemodynamics. For example, the connection between peripheral ischemia and small thermal variations has been demonstrated in a number of previous research. To the best of our knowledge, there are no freely accessible, open-source programs to perform dynamic thermal analysis and processing to evaluate peripheral perfusion in the human body. In addition, such tools supporting dynamic measurement setups, such as thermal modulation tests do not exist. Computational methods implemented in IRlab could provide a useful and easily accessible framework and individual computational components for researchers within the field of medical thermal imaging. Although there are known limitations, such as registration and speed optimization and unknown limitations, IRlab is an ongoing open-source project and community needs and reported issues are taken into account during further development. The proposed software allows the user to perform standard analysis and processing methods, along with novel dynamic measures combined with thermal modulation tests. IRlab is intended mainly for PAD, and more specifically in CLTI research, but the software may be used for other part within the body. We emphasize that IRlab is intended only to be used as a research tool under the GPL, and should not be used in clinical practice.

Declaration of competing interest

The authors declare that they have no known competing financial interests or personal relationships that could have appeared to influence the work reported in this paper.

Acknowledgements

Authors have no competing interest to declare. This research was funded by the Instrumentarium Science Foundation, Finland, as a

personal grant for Tomppa Pakarinen's doctoral research, and by State Research Funding (VTR), Finland.

References

[1] Subramaniam Bagavathiappan, Saravanan Thangavelu, Philip John, Jayakumar T, Raj Baldev, Rajamanickam Karunanithi, Panicker T, Korath M, Jagadeesan K. Infrared thermal imaging for detection of peripheral vascular disorder. J Med Phys 2009;34:43–7. https://doi.org/10.4103/0971-6203.48720.

[2] Peregrina-Barreto H, Morales-Hernández L, Rangel-Magdaleno J, Avina-Cervantes J, Ramirez-Cortes J, Morales-Caporal R. Quantitative estimation of temperature variations in plantar angiosomes: a study case for diabetic foot. Comput Math Methods Med 2014:585306. https://doi.org/10.1155/2014/585306.

[3] Sagaidachnyi A, Fomin A, Usanov D, Skripal A. Thermography-based blood flow imaging in human skin of the hands and feet: a spectral filtering approach. Feb Physiol Meas 2017;38(2):272–88. https://doi.org/10.1088/1361-6579/aa4eaf. Epub 2017 Jan 18. PMID: 28099162.

[4] Gerhard-Herman M, et al. 2016 AHA/ACC guideline on the management of patients with lower extremity peripheral artery disease. Circulation 2017;135:e686–725.

[5] Mori Taketoshi, Nagase Takashi, Takehara Kimie, Oe Makoto, Ohashi Yumiko, Amemiya Ayumi, Noguchi Hiroshi, Ueki Kohjiro, Kadowaki Takashi, Sanada Hiromi. Morphological pattern classification system for plantar thermography of patients with diabetes. J.Diabetes.Sci. Technol. 2013;7:1102–12. https://doi.org/10.1177/193229681300700502.

[6] Gatt A, Falzon O, Cassar K, Ellul C, Camilleri K, Gauci J, Mizzi S, Mizzi A, Sturgeon D, Cassandra, Camilleri L, Chockalingam N, Formosa C. Establishing differences in thermographic patterns between the various complications in diabetic foot disease. Int. J. Endocrinol. 2018:1–7. https://doi.org/10.1155/2018/9808295. 2018.

[7] Rother U, Lang W, Horch RE, Ludolph I, Meyer A, Gefeller O, Regus S. Pilot assessment of the angiosome concept by intra-operative fluorescence angiography after tibial bypass surgery. Feb Eur J Vasc Endovasc Surg 2018;55(2):215–21. https://doi.org/10.1016/j.ejvs.2017.11.024. Epub 2018 Jan 3. PMID: 29305093.

[8] Seixas A, Ammer K, Carvalho R, Vilas-Boas JP, Vardasca R, Mendes J. Skin temperature in diabetic foot patients: a study focusing on the angiosome concept. In: Tavares J, Natal Jorge R, editors. VipIMAGE 2017. ECCOMAS. Lecture notes in computational vision and biomechanics, vol. 27. Cham: Springer; 2018. https://doi.org/10.1007/978-3-319-68195-5_114.

[9] Huang TY, Huang TS, Wang YC, Huang PF, Yu HC, Yeh CH. Direct revascularization with the angiosome concept for lower limb ischemia: a systematic review and meta-analysis. Aug Medicine (Baltim) 2015;94(34):e1427. https://doi.org/10.1097/MD.0000000000001427. PMID: 26313796; PMCID: PMC4602934.

[10] Sumpio B, Forsythe R, Ziegler K, van Baal J, Lepantalo M, Hinchliffe R. Clinical implications of the angiosome model in peripheral vascular disease. Sep J Vasc Surg 2013;58(3):814–26. https://doi.org/10.1016/j.jvs.2013.06.056. PMID: 23972249.

[11] Kaczmarek M, Nowakowski A. Active IR-thermal imaging in medicine. J Nondestr Eval 2016;35. https://doi.org/10.1007/s10921-016-0335-y.

[12] Soliz P, et al. Detection of diabetic peripheral neuropathy using spatial-temporal analysis in infrared videos. In: 50th asilomar conference on signals, systems and computers, 2016; 2016. p. 263–7. https://doi.org/10.1109/ACSSC.2016.7869038.

[13] Geyer M, Yih-Kuen J, Brienza D, Boninger M. Using wavelet analysis to characterize the thermoregulatory mechanisms of sacral skin blood flow. J Rehabil Res Dev 2004;41:797–806. https://doi.org/10.1682/JRRD.2003.10.0159.

[14] Sagaidachnyi A, Volkov I, Fomin A. In: Influence of temporal noise on the skin blood flow measurements performed by cooled thermal imaging camera: limit possibilities within each physiological frequency range", Proc. SPIE 9917, Saratov Fall Meeting 2015: third International Symposium on Optics and Biophotonics and Seventh Finnish-Russian Photonics and Laser Symposium (PALS), 99170N; 2016. https://doi.org/10.1117/12.2229476. 21 April.

[15] Zadeh G, Hamidreza J, Farshad N, Bijan R. In: The application of wavelet transform in diagnosing and grading of varicocele in thermal images: the selected papers of the first international conference on fundamental research in electrical engineering; 2019. https://doi.org/10.1007/978-981-10-8672-4_11.

[16] Chang K, Yoon S, Sheth N, Seidel M, Antalek M, Ahad J, Darlington T, Ikeda A, Kato GJ, Ackerman H, Gorbach AM, Rapid vs. Delayed infrared responses after ischemia reveal recruitment of different vascular beds. Quant InfraRed Thermogr J 2015;12(2):173–83. https://doi.org/10.1080/17686733.2015.1046677. Epub 2015 Jun 16. PMID: 26435756; PMCID: PMC4589278.

[17] Tze-Yuan C, Cila H. Motion tracking in infrared imaging for quantitative medical diagnostic applications. Infrared Phys Technol 2013;62. https://doi.org/10.1016/j.infrared.2013.10.009.

[18] Liu G, Liu Z, Liu S, et al. Registration of infrared and visible light image based on visual saliency and scale invariant feature transform. J Image Video Proc 2018;45. https://doi.org/10.1186/s13640-018-0283-9.

[19] González-Pérez S, Perea Ström D, Arteaga-Marrero N, Luque C, Sidrach-Cardona I, Villa E, Ruiz-Alzola J. Assessment of registration methods for thermal infrared and visible images for diabetic foot monitoring. Sensors 2021;21(7):2264. https://doi.org/10.3390/s21072264.

[20] Gorbach A, Ackerman H, Liu W, Meyer J, Littel P, Seamon C, Footman E, Chi A, Zorca S, Krajewski M, Cuttica M, Machado R, Cannon R, Kato G. Infrared imaging of nitric oxide-mediated blood flow in human sickle cell disease. Nov Microvasc Res 2012;84(3):262–9. https://doi.org/10.1016/j.mvr.2012.06.011. Epub 2012 Jul 8. PMID: 22784510; PMCID: PMC3483464.

[21] Gorbach AM, Wang H, Elster E. Thermal oscillations in rat kidneys: an infrared imaging study. Philos. Trans. R. Soc. A Math. Phys. Eng. Sci. 2008;366:3633–47.

[22] Bharara M, Viswanathan V, Cobb JE. Cold immersion recovery responses in the diabetic foot with neuropathy. Oct Int Wound J 2008;5(4):562–9. https://doi.org/10.1111/j.1742-481X.2008.00454.x. pub 2008 Sep 1. PMID: 18783470.

[23] Fujiwara Y, Inukai T, Aso Y, Takemura Y. Thermographic measurement of skin temperature recovery time of extremities in patients with type 2 diabetes mellitus. 2000.

[24] Matlab. Version 9.8 (R2020b. Natick, Massachusetts: The MathWorks Inc; 2020.

[25] Budzan S, Wyżgolik R. Remarks on noise removal in infrared images. Measurement Automation Monitoring 2015;61:187–90.

[26] Hanson C. In: Implications of 1/f noise in uncooled thermal imaging", Proc. SPIE 10624, Infrared Technology and Applications XLIV, 106241C; 2018. https://doi.org/10.1117/12.2306334.

[27] Low D, Harms W, Mutic S, Purdy J. A technique for the quantitative evaluation of dose distributions. Med Phys 1998;25(5):656–61. https://doi.org/10.1118/1.598248. PMID: 9608475.

[28] Geurts M. CalcGamma, GitHub repository. Available at: https://github.com/mwgeurts/gamma; 2014. 5.8.2020.

[29] Alexandrescu V, Söderström M, Venermo M. Angiosome theory: fact or fiction? Scand J Surg 2012;101(2):125–31. https://doi.org/10.1177/145749691210100209. PMID: 22623446.

[30] Pakarinen T, Pietilä J, Nieminen H. Prediction of self-perceived stress and arousal based on electrodermal activity *. In: Conference proceedings: annual international conference of the IEEE engineering in medicine and biology society. IEEE engineering in medicine and biology society. Conference; 2019. p. 2191–5. https://doi.org/10.1109/EMBC.2019.8857621. 2019.